Commun. Comput. Phys.
doi: 10.4208/cicp.150915.170316a

Vol. **20**, No. 3, pp. 660-688
September 2016

Particle Methods for Viscous Flows: Analogies and Differences Between the SPH and DVH Methods

Andrea Colagrossi[1,*], Emanuele Rossi[1,2], Salvatore Marrone[1,2] and David Le Touzé[2]

[1] *CNR-INSEAN, Marine Technology Research Institute, Rome, 00128, Italy.*
[2] *Ecole Centrale Nantes, LHEEA Lab. (UMR CNRS), Nantes, France.*

Received 15 September 2015; Accepted (in revised version) 17 March 2016

Abstract. In this work two particle methods are studied in the context of viscous flows. The first one is a Vortex Particle Method, called Diffused Vortex Hydrodynamics (DVH), recently developed to simulate complex viscous flows at medium and high Reynolds regimes. This method presents some similarities with the SPH model and its Lagrangian meshless nature, even if it is based on a different numerical approach. Advantages and drawbacks of the two methods have been previously studied in Colagrossi et al. [1] from a theoretical point of view and in Rossi et al. [2], where these particle methods have been tested on selected benchmarks. Further investigations are presented in this article highlighting analogies and differences between the two particle models.

PACS: 47.11.-j, 47.32.C-, 47.54.-r

Key words: Particle methods, meshless methods, vortex methods, Smoothed Particle Hydrodynamics (SPH), Diffused Vortex Hydrodynamics (DVH).

1 Introduction

This work is addressed to the analysis of two particle methods: the Smoothed Particle Hydrodynamics (SPH) and the Diffused Vortex Hydrodynamics (DVH). The latter is a Vortex Particle Method (VPM) recently presented in Rossi et al. [2] and validated on classical viscous flows around bodies in Rossi et al. [3].

The basic concepts underlying the SPH and the VPM have been previously studied in Colagrossi et al. [1] were the main focus was on the theoretical aspects of two particle methods. More recently in Rossi et al. [2] the DVH method has been introduced and compared with the SPH model in terms of similarities on the convergence properties of

*Corresponding author. *Email addresses:* andrea.colagrossi@cnr.it (A. Colagrossi), erossi.vortex@gmail.com (E. Rossi), salvatore.marrone@cnr.it (S. Marrone), david.letouze@ec-nantes.fr (D. Le Touzé)

 ©2016 Global-Science Press

https://doi.org/10.4208/cicp.150915.170316a Published online by Cambridge University Press

the two schemes. In the present work the investigation on these two particle methods has been extended by completing some lacking points of the research.

To better focus the framework of the current investigation, a classification in four families of the most popular Navier-Stokes Lagrangian solvers is reported in Table 1. The advantages in using Lagrangian solver is mainly in the treatment of the direct advection of the particles which leads to a reduction of the numerical dissipation with respect to mesh based approaches. The first subdivision of Table 1 is based on the primary variables adopted: pressure-velocity or vorticity fields.

Table 1: A possible classification of the most popular Navier-Stokes Lagrangian solvers.

	Pressure & Velocity	**Vorticity** (VPM)
Need topological connections (for evaluating spatial derivatives)	P-FEM, α-NEM, PIC (Particle in Cell), FLIP (Fluid - Particle in cell [4]) Voronoi moving mesh	VIC (Vortex in Cells), Remeshed-Vortex-Method
Meshless approach (use of Kernel convolutions)	SPH, ISPH (incompressible SPH), MPS (Moving Particle Semi-implicit method), FVPM (Finite Volume Particle Method)	DVH, PSE (Particle Strength Exchange), DVM (Diffused Velocity Method), VVD (Viscous Vortex Domains method), VRM (Vorticity Redistribution Method), RVM (Random Vortex Method)

The use of the vorticity as a primary variable brings several advantages when solving the Navier-Stokes equation for incompressible flows:

1. the pressure field is not a direct unknown of the problem,
2. the continuity equation is automatically satisfied,
3. the vorticity formulation allows to discretize only the rotational region of the flow (self-adaptivity),
4. high accuracy on the evaluation of the velocity field (because it is obtained through a spatial integration),
5. the boundary conditions at infinity are automatically satisfied, therefore large spatial domains are not required to correctly enforce them.

These points represent the main differences between VPM and the Pressure-Velocity based Lagrangian solvers. For the latter the velocity-divergence constraint need to be explicitly handled, requiring the discretization of the whole fluid domain. Moreover, the radiation boundary conditions cannot be imposed easily in these methods, implying the use of very large domains. On the other hand the Pressure-velocity Lagrangian solvers have the advantage of a direct evaluation of the fluid deformation in the whole domain which can be quite useful for many engineering/industrial applications. For example

https://doi.org/10.4208/cicp.150915.170316a Published online by Cambridge University Press

with the SPH method it is easy to give different fluid properties to different sets of particles (few changes are needed) while this operation is generally not straightforward using vortex methods.

The second subdivision reported in Table 1 regards whether the method uses or not a mesh for the evaluation the spatial derivatives. In VPM methods generally a Fast Multiple Method (FMM) approach is used for the evaluation of the velocity induced by the vortex particles, allowing for a complete mesh-free approach. In other approaches like Vortex-in-Cells and Remeshed-Vortex-Method, the vortex particles are interpolated at each time step on a mesh and the Poisson equation, which links the velocity to the vorticity field, is evaluated on this grid by calculating the spatial derivatives on mesh nodes. The benefits of using FMM techniques are: (i) the availability of very efficient HPC algorithms, (ii) spatial multi-resolutions can be handled in a simple way. Concerning the latter item, this is not the case for the Pressure-Velocity Lagrangian method where the pressure-force interactions in a multi-resolution context requires specific numerical treatments (see *e.g.* [5]).

The present article starts with a comparison between the SPH and VPM schemes in the framework of inviscid flows (Euler equation (2.1)) where the discussion on some crucial numerical similarities and differences of the two methods can be easily handled. In Section 2.2 the viscous flows context is considered. Here the DVH method is introduced for its ability in taking into account the viscous diffusion process with respect to other VPM methods. In the DVH method the classical splitting algorithm conceived by Chorin (1973) [6] is used, thus allowing to write the time integration as a superimposition of diffusion and advection steps. During a diffusion step each vortex particle gives a vorticity contribution on a suitable set of points through the elementary solution of the heat equation. This particular way of solving the diffusion process is rather similar to the smoothing procedure employed in the SPH method, which leads to a convergence behaviour very similar to the one discussed in the literature (see *e.g.* [7] and [8]). Both SPH and DVH approaches employ explicit time integration for the particle system advection. A discussion on the time integration schemes of these two models is provided in Section 3. In Section 4 two numerical test-cases are presented to better show the different points discussed in the article from a practical point of view. Finally, in Section 5 similarities and differences between SPH and DVH are summarized after considering the analysis presented in the previous sections.

2 Vortex Particle Method (VPM) vs SPH

2.1 Inviscid flows

In the SPH method a fluid domain Ω of total mass M is discretized in N particles, m_i being the mass of the generic i-th particle. Conversely in VPMs a vorticity field, with total circulation Γ, is discretized in N vortex particles, where the ith vortex is associated to the circulation Γ_i. Therefore, during the time evolution, the SPH guarantees the mass conser-

https://doi.org/10.4208/cicp.150915.170316a Published online by Cambridge University Press

vation $M=\sum_i m_i$ while VPMs conserve the total circulation $\Gamma=\sum_i \Gamma_i$. In both the methods a mollification procedure with a kernel function W is used to obtain a continuous field from the particle set in the whole domain:

$$\begin{aligned} &\text{SPH:} \quad \langle\rho\rangle(\boldsymbol{r}) = \sum_j m_j W(\boldsymbol{r}_j - \boldsymbol{r};\epsilon), \\ &\text{VPM:} \quad \langle\omega\rangle(\boldsymbol{r}) = \sum_j \Gamma_j W(\boldsymbol{r}_j - \boldsymbol{r};\epsilon), \end{aligned} \tag{2.1}$$

where ϵ is the specific smoothing length adopted. Hence, density and vorticity are the two smoothed fields in these methods.

Another smoothing procedure can be expressed to directly evaluate density or vorticity on the particle positions $\boldsymbol{r}_i$ (see *e.g.* [9]):

$$\begin{aligned} &\text{SPH:} \quad \langle\rho\rangle(\boldsymbol{r}_i) = m_i \sum_j W_{ij}, \\ &\text{VPM:} \quad \langle\omega\rangle(\boldsymbol{r}_i) = \Gamma_i \sum_j W_{ij}, \end{aligned} \tag{2.2}$$

where $W_{ij}=W(\boldsymbol{r}_j-\boldsymbol{r}_i;\epsilon)$ for the sake of brevity. In Eq. (2.2) it is more clear the role of the kernel function W in evaluating the volume ΔV_i occupied by the mass or the circulation of the generic i-th particle. In both smoothing procedures the functions $\langle\rho\rangle$ and $\langle\omega\rangle$ are largely affected by:

1. the smoothing length ϵ,
2. the mean particle distance $\Delta r=(\Delta V_i)^{1/n}$ ($n=2$ in 2D),
3. the regularity of particle spatial positions (see *e.g.* [10]).

In this work the adopted kernel function W for the SPH models is the Wendland C2 [11] with compact support of radius equal to $R_w=2\epsilon$. As for the VPM, usually a kernel with infinite support is adopted, like (see *e.g.* [12]):

$$W(r) := \frac{2}{\pi\epsilon^2} \frac{1-\left(r/\epsilon\right)^2}{\left[1+\left(r/\epsilon\right)^2\right]^4}. \tag{2.3}$$

We recall that the ratio $\epsilon/\Delta r$ is a key parameter for the accuracy and rate of convergence of the smoothing procedure. For practical applications $\epsilon/\Delta r=2$ can be considered a good compromise for both the VPM and the SPH.

Starting from the similarity of the smoothing procedures (2.1) and (2.2), already well underlined and discussed in the literature (*e.g.* [13]), important differences arise when these are employed in the governing fluid equation. If one considers for the SPH a non-dissipative motion of fluid particles, the momentum equation directly comes from Lagrange's equations when using the mollified density distribution $\langle\rho\rangle$ (see *e.g.* [14]). This

https://doi.org/10.4208/cicp.150915.170316a Published online by Cambridge University Press

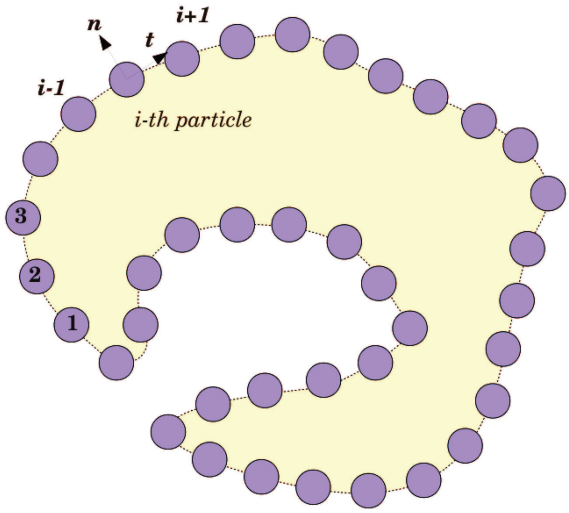


Figure 1: A necklace made by a set of SPH particles for the evaluation of circulation through Eq. (2.5).

implies that the kernel function W enters in the particle acceleration through the pressure-forces interaction, *i.e.*:

$$\begin{cases} \dfrac{D\boldsymbol{u}_i}{Dt} = -m_i \displaystyle\sum_j \left(\frac{p_i}{\rho_i^2} + \frac{p_j}{\rho_j^2} \right) \nabla_i W_{ij}, \\ \dfrac{D\boldsymbol{r}_i}{Dt} = \boldsymbol{u}_i, \qquad p_i = f(\rho_i), \qquad \rho_i = \displaystyle\sum_j m_j W_{ij}, \end{cases} \tag{2.4}$$

where ∇_i indicates the differentiation with respect to the position of the i-th particle. A peculiarity of the SPH method is that the symmetry of the Lagrangian and the continuity equation lead to the conservation of the energy and the linear and angular momenta.

It is possible to show that in isentropic conditions also the circulation Γ_l of an arbitrary loop l of particles, evaluated as:

$$\Gamma_l = 1/2 \sum_{i \in l} \boldsymbol{u}_i \cdot (\boldsymbol{r}_{i+1} - \boldsymbol{r}_{i-1}), \tag{2.5}$$

is preserved if particle masses are identical (see Fig. 1). This property can be considered a further common feature between SPH and VPM. However, if complex flows are considered, the material loop l of particles can be destroyed during the evolution and the control on the circulation become meaningless (for details see [15]). Being the circulation a primary variable of the particle system, this problem does not arise in the VPM method.

For the VPMs, the Euler equation need to be re-shaped using vorticity field instead of

https://doi.org/10.4208/cicp.150915.170316a Published online by Cambridge University Press

pressure-velocity ones:

$$\boxed{\text{2D Euler equation}}\begin{cases}\dfrac{D\omega(\mathbf{r},t)}{Dt}=0,\\ \dfrac{D\mathbf{r}}{Dt}=\mathbf{u}(\mathbf{r},t),\\ \nabla^2\mathbf{u}(\mathbf{r},t)=-\text{curl}(\omega\mathbf{e}_3),\end{cases} \tag{2.6}$$

which, for a finite number of vortex particles, becomes:

$$\begin{cases}\dfrac{D\Gamma_i}{Dt}=0,\\ \dfrac{Dr_i}{Dt}=\boldsymbol{u}_i,\\ \boldsymbol{u}(\boldsymbol{r}_i)=\displaystyle\sum_j\Gamma_j\boldsymbol{K}_{ij},\quad \boldsymbol{K}_{ij}:=-\frac{1}{2\pi}\mathbf{e}_3\times\frac{(\boldsymbol{r}_i-\boldsymbol{r}_j)}{|\boldsymbol{r}_i-\boldsymbol{r}_j|^2},\end{cases} \tag{2.7}$$

where $\mathbf{e}_3$ is the normal unit vector orthogonal to the fluid domain plane. The vortex particles interact with each other according the well known Biot-Savart law which gives the velocity field induced by the circulation Γ_j of the particles through the Kernel function $\boldsymbol{K}_{ij}$.

It is important to note that Eq. (2.7) does not depend by the Kernel W, which is needed only to evaluate the vorticity field through Eq. (2.1). However, in order to avoid numerical singularities when two vortices nearing too much close the Kernel $\boldsymbol{K}$ can be regularized through the smoothing procedure:

$$\boldsymbol{K}_\epsilon(\boldsymbol{r}-\boldsymbol{r}')=\int_\Omega W(r-r^*;\epsilon)\boldsymbol{K}(r^*-r')dr^* \tag{2.8}$$

and the new kernel $\mathbf{K}_\epsilon$ can be used in (2.7) replacing $\boldsymbol{K}$ (see e.g. [16]).

Summarising, for the VPM the smoothed vorticity $\langle\omega\rangle$ is evaluated through a post-processing, and the kernel W affects the motion of vortex particle only through the dependency of the kernel $\mathbf{K}_\epsilon$. The latter function has a totally different behaviour with respect to ∇W: in fact, $\mathbf{K}_\epsilon$ has a long-range influence while ∇W has a short-range action, affecting only particles close enough. This difference implies the use of distinct algorithms for the particle interactions: in the SPH a neighbour-linked-list [17] can be usually adopted whereas in the VPM a hierarchical calculation algorithm is needed [18].

The use of an oct-tree algorithm allows an increase of the computational efficiency for the evaluation of the "Biot-Savart" summation (Eq. (2.7)), through the fast multipole methods (FMM). In the FMM the computational domain is recursively divided into panels, until every panel contains a number of vortices not greater than a certain threshold (in this work this number is 200). While constructing the domain subdivisions, the panels are ordered in a hierarchical tree structure. Going across the panels, the velocity of each

https://doi.org/10.4208/cicp.150915.170316a Published online by Cambridge University Press

vortex is calculated using the Biot-Savart summation to account for the interaction with the vortices in the nearest neighbours of the actual panel, while the effect of the other vortices are approximated using a multipole expansion (see *e.g.* [19]).

A second important point related to the particle interactions is the handling of multi-resolution. Left plot of Fig. 2 shows an example of a multi-resolution vortex particle distribution. In this figure three different zones are present: zone 1 – coarse resolution, zone 2 – fine resolution, zone 3 mixing between the two different sets of particles. Middle plot of Fig. 2 depicts the velocity streamline obtained using Eq. (2.7). From this result it is possible to see that the velocity field is not largely affected neither by the change of the resolution nor by the particle disorder. Conversely, for the SPH the pressure-force interactions among particles of different size requires specific numerical treatments (see *e.g.* [5,20–22]).

Both the SPH and the VPM schemes (Eqs. (2.4) and (2.7)) for inviscid flows present numerical issues. The SPH suffers from numerical instabilities mainly linked to the explicit time integration schemes adopted and to the very low level of numerical diffusion. Therefore, usually artificial diffusion terms are added in Eq. (2.4) (see *e.g* [23–26]). In addition, the state of stress (e.g. tensile instability [27]) and rank deficiency (zero-energy modes) instabilities, arising from utilization of Eulerian kernels in Lagrangian descriptions of particles' motion (e.g. [28]), and approximations of field variables and their derivatives at the same calculation points [29], are respectively known to be among famous instabilities seen in SPH context. Some details on how it is possible to control such instabilities in are given in [8,30–32]).

From the VPM side the main problem when dealing with an inviscid simulation is that the particle distribution may become irregular during the time evolution (see *e.g.* Fig. 3). For this reason a remeshing procedure is generally adopted to interpolate the particle data over a regular distribution of points, which on the other hand introduces a numerical dissipation (see *e.g.* [33]).

Usually, the interpolation formula adopted for the remeshing procedure allows to conserve the circulation as well as the linear and angular momentum of the vorticity field. In some VPMs the remeshing is performed at each time step; this means that the particles are always on a regular mesh and, therefore, the volume ΔV_i occupied by the i-th particle is known. In such a condition, the vorticity can be simply evaluated through

$$\omega(\boldsymbol{r}_i) = \frac{\Gamma_i}{\Delta V_i} \tag{2.9}$$

without any need for smoothing procedure (Eq. (2.1) or (2.2)). Furthermore, since particles are on a mesh, the Poisson equation for the velocity field (last equation of (2.6)), can be evaluated through an efficient mesh-based solver. Therefore, the FMM is not necessary any more as well as the use of a regularized kernel $\boldsymbol{K}_\epsilon$. These VPMs are not pure meshless methods and the main errors of the scheme come from the re-meshing procedure and from the Poisson solver; in this sense the analogies with the SPH are almost completely lost.

https://doi.org/10.4208/cicp.150915.170316a Published online by Cambridge University Press

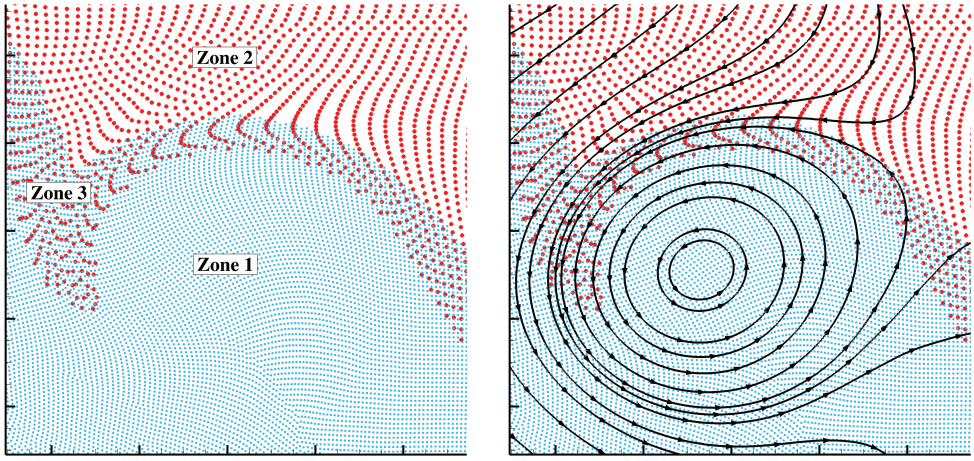


Figure 2: Multi-resolution in Vortex Particle Method: example of a vortex particle distribution (left), velocity streamlines evaluated through Eq. (2.7) (right).

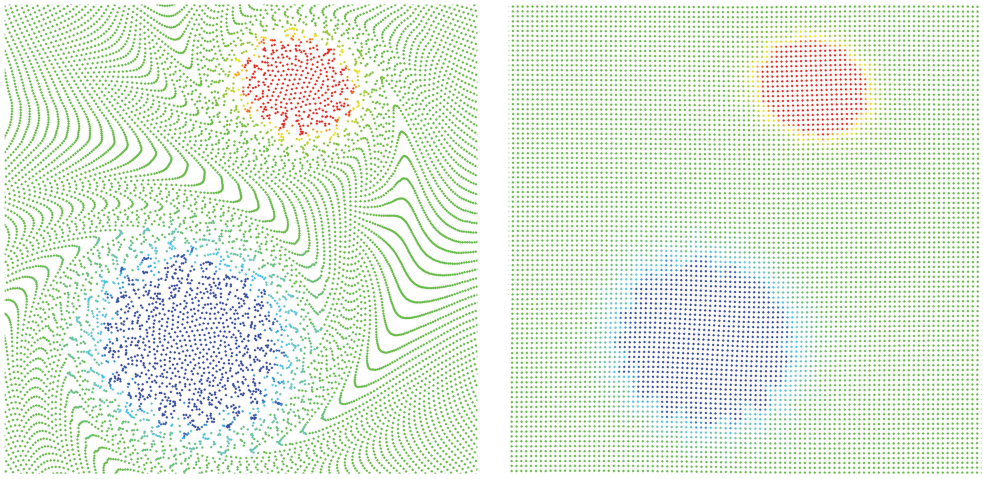


Figure 3: Vortex Particle distribution during the inviscid evolution of two vortex blobs, before remeshing (left), after remeshing (right).

In the next section, we show how in the DVH scheme the particle redistribution procedure can be embedded directly in the viscous dissipation (as in other meshless VPMs see *e.g.* [34]). Thanks to this approach, similarities with the SPH are still preserved.

2.2 Viscous flows

2.2.1 Diffused Vortex Hydrodynamics

In this section the Navier-Stokes equation for a 2D incompressible flow, written in vorticity ω is considered:

https://doi.org/10.4208/cicp.150915.170316a Published online by Cambridge University Press

$$\boxed{\text{2D N.S. equation}} \begin{cases} \dfrac{D\omega(\mathbf{r},t)}{Dt} = \nu\nabla^2\omega, \\ \dfrac{D\mathbf{r}}{Dt} = \mathbf{u}(\mathbf{r},t), \\ \nabla^2\mathbf{u}(\mathbf{r},t) = -\text{curl}(\omega\mathbf{e}_3). \end{cases} \tag{2.10}$$

According to the Chorin's operator splitting scheme the numerical solution is obtained by solving an inviscid advection step followed by a purely diffusive one. The first one has been described in the previous section and Eq. (2.7) are solved using a FMM method.

During the diffusive step the fluid is considered at rest and the vorticity diffusion is obtained by solving the linear "heat equation":

$$\frac{\partial\omega}{\partial t} = \nu\nabla^2\omega. \tag{2.11}$$

In the DVH scheme this second step is solved by using a deterministic diffusion algorithm described in [35] and briefly recalled in the following. The presence of a body within the flow field requires the generation of vorticity on the solid walls because of the no-slip boundary condition. This is achieved by adding an appropriate process between the advection and the diffusion steps (see *e.g.* [3]). Concerning the evaluation of the hydrodynamic loads acting on the solid body, the procedure described in [1] is adopted.

Regarding the diffusion process, we start considering a single vortex particle with position $\mathbf{r}_i$ and strength Γ_i. The analytical solution of the heat equation (2.11) for this single particle can be expressed at time $t = t_0 + \Delta t_d$ as:

$$\begin{cases} \omega(\mathbf{r},t_0+\Delta t_d) = \dfrac{\Gamma_i}{4\pi\nu\Delta t_d}\exp\left[-\dfrac{(r-r_i)^2}{4\nu\Delta t_d}\right] & \text{if } |\mathbf{r}-\mathbf{r}_i| \le R_d, \\ \omega(\mathbf{r},t_0+\Delta t_d) = 0 & \text{otherwise,} \end{cases} \tag{2.12}$$

where the Gaussian distribution has been truncated at distance R_d for numerical purpose. R_d is called "diffusive radius" and it is a key parameter of the convergence properties of the DVH scheme as discussed in the next sections.

Right plot of Fig. 4 shows a single vortex and its diffusive radius, during the diffusion time step. Following [35], the vorticity is spread around it using Eq. (2.12) and a new circulation distribution can be assigned to a new set of points belonging to a regular stencil, characterized by a resolution length Δr. At the end of the diffusive time step these geometrical points become the new set of vortex particles. In case of free-vorticity dynamics the stencils can be regular tessellations of the 2D plane (see [2]) or an ad-hoc distribution like the one shown in the left plot of Fig. 4, which has been obtained using the packing algorithm described in [36]. The latter allows for a regularization of the point distribution around an object with generic shape. The distribution comes back to a regular tessellation for a distance large enough from solid surfaces. Finally a renormalization procedure is used to preserve the conservation of the circulation given by each vortex (see [2]).

https://doi.org/10.4208/cicp.150915.170316a Published online by Cambridge University Press

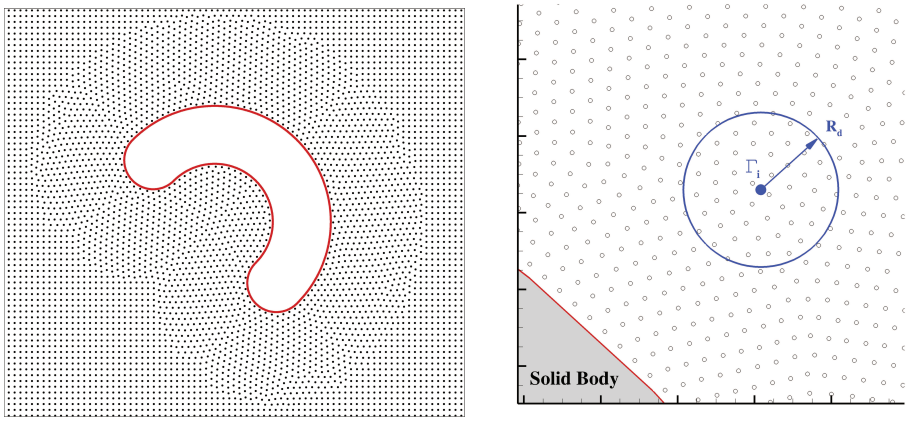


Figure 4: Regular stencil used for the diffusion process around a generic object obtained through a packing algorithm [36] (left). Enlarged view around a single vortex with its diffusive radius R_d (right).

The spreading of the vorticity on a new set of points resemble the classical re-meshing procedure usually adopted in the VPMs. Conversely, in the DVH an interpolation is not needed since a physical process is used to redistribute both the vorticity field and the circulation.

The use of a truncated Gaussian distribution for the diffusion step introduces again an analogy with the SPH smoothing procedure. Indeed, we show in the following sections that the diffusive radius plays the same role of the kernel support radius $R_w = 2\epsilon$ on the convergence behaviour of the DVH. This analogy becomes stronger when considering that an optimum value for the ratio $R_d/\Delta r$ is around 4 which is the same ratio $R_w/\Delta r$ used in the SPH with the Wendland C2 kernel.

2.2.2 Viscous flows with SPH

In this subsection a brief recall of how viscous flows can be treated in the SPH framework is reported. In the literature there are different SPH formulations of the viscous term. Among these the most classical ones are, respectively, by Monaghan and Gingold [37] and by Morris et al. [38]. Assuming that the viscosity coefficients are constant all over the fluid domain, the Monaghan & Gingold formulation of the viscous term is:

$$\langle \nabla \cdot \mathbb{V} \rangle_i = \mu \sum_j \frac{m_j}{\rho_j} \pi_{ij} \nabla_i W_{ij}, \qquad \pi_{ij} := K \frac{(\boldsymbol{u}_j - \boldsymbol{u}_i) \cdot (\boldsymbol{r}_j - \boldsymbol{r}_i)}{|\boldsymbol{r}_j - \boldsymbol{r}_i|^2}, \tag{2.13}$$

where $\mathbb{V}_i$ is the viscous tensor evaluated on the particle i-th position. and K is a parameter depending on the spatial dimension ($K = 6,8,10$, respectively in $1D$, $2D$ and $3D$). Using the relations found by Español and Revenga [39] for the estimation of the second derivatives in SPH, inside the domain this formulation is consistent as:

$$\lim_{\epsilon \to 0, \frac{\Delta r}{\epsilon} \to 0} \langle \nabla \cdot \mathbb{V} \rangle = \mu \nabla^2 \boldsymbol{u} + 2\mu \nabla (\nabla \cdot \boldsymbol{u}). \tag{2.14}$$

https://doi.org/10.4208/cicp.150915.170316a Published online by Cambridge University Press

The last term is the viscosity dissipation linked with the compressibility of the media. In the context of weakly compressible flows this term plays a negligible role as shown in *e.g.* [40, 41]. Besides the drawback of having a compressible viscous term that induces a non-null bulk viscosity, the formulation (2.13) has the advantage of guaranteeing the conservation of both linear and angular momenta for the particle system, thanks to the property that $\sum_i m_i \langle \nabla \cdot \mathbb{V} \rangle_i / \rho_i$ is invariant for Galilean transformation. This global properties can play a non-negligible role in some conditions as remarked in [42] and for this reason the formula (2.13) is adopted in this work. A general discussion on the dissipative forces for Lagrangian models is presented in [43] where the author shows that both Eq. (2.13) and the Kernel function W adopted here satisfy the requirements to get a correct treatment of dissipative forces in Lagrangian methods, in connection to the principles of Hamiltonian and statistical mechanics.

Comparing the SPH viscous diffusion with the DVH one, one can observe that Eq. (2.13) depends mainly on the positions and velocities of the particles that are inside the kernel support R_w. Similarly to what discussed for the DVH, also in the SPH a constraint on the time step Δt_d arises in order to avoid that the diffusion propagation in a Δt_d becomes too large with respect to R_w, i.e.

$$\sqrt{\nu \Delta t_d} < R_w.$$

On the other hand in the DVH method the diffusion process is not directly linked to the vortex particle positions since the diffusion of the vorticity field is performed on a regular distribution of geometrical points. This is an advantage since the diffusion process is not affected by the irregularities of the vortex spatial configuration. This is not the case for the SPH method where large numerical errors can be induced by disordered particle distributions (see [10]). Therefore, in enhanced versions of the SPH method different corrections have been proposed (see *e.g.* [44], [45]) to overcome this drawback. Besides these corrections another way to limit this error may be the increase of the number of particles inside the kernel support R_w, as further discussed in Section 4.

The other advantage of the DVH is that the diffusion is performed directly on the vorticity while in SPH a second order operator for the velocity field is needed and it is based on a low order integral interpolation formula. As already pointed out, the accuracy of second order operators is quite sensitive to the particle disorder. Indeed, considering a simple linear velocity field, formula (2.13) is not able to recover null value of $\langle \nabla \cdot \mathbb{V} \rangle$ for a generic particle distribution.

3 Time integration in the DVH and in the SPH models

In the present section the time integrations of the DVH and SPH models is discussed. For both methods an explicit integration based on a fourth-order Runge-Kutta scheme is adopted. This limits the range of applicability of these solvers. Indeed, the explicit integration of high viscous flow simulations ($\mathrm{Re} < 1$) implies very small time steps (as

https://doi.org/10.4208/cicp.150915.170316a Published online by Cambridge University Press

further explained in details). The SPH and DVH are, therefore, not suitable to deal with this kind of flow, unless the diffusion process is solved through implicit integration.

Following the derivation described in [2] the time step for the diffusion process is given by:

$$\Delta t_d = 0.021 \frac{R_d^2}{\nu}. \tag{3.1}$$

Re-arranging the above equation using non-dimensional variables and fixing the ratio $R_d/\Delta r = 4$, it is possible to relate the diffusive time step Δt_d to the spatial resolution $L/\Delta r$ and the Reynolds number:

$$\Delta t_d \frac{U}{L} = 0.021 \frac{\mathrm{Re}}{(L/R_d)^2} \simeq 0.34 \frac{\mathrm{Re}}{(L/\Delta r)^2} = 0.34 \frac{\mathrm{Re}_{\Delta r}}{(L/\Delta r)}, \tag{3.2}$$

where L is the length scale of the specific problem at hand and $\mathrm{Re}_{\Delta r} = U\Delta r/\nu$ the so-called Reynolds cell. The latter needs to be $\mathcal{O}(1)$ at least in the region of main interest in order to properly simulate all the vorticity scales.

Together with the diffusive time step one needs to consider also the time step, Δt_a, for the advection of the particles. This can be chosen by considering the flow velocity U and the discretization Δr of the stencil used during the diffusion step. A first evaluation of Δt_a can be chosen as:

$$\Delta t_a \frac{U}{L} = K_1 \frac{1}{(L/\Delta r)}, \tag{3.3}$$

where K_1 is a number which should be of order $\mathcal{O}(10^{-1})$ to avoid too large displacements during the advection steps which can results in disordered particle configurations (values between 0.1 and 1.5 have been used in the simulations presented in Section 4).

It is important to underline that the time steps (3.2), (3.3) are constrained only for accuracy and not for stability purpose (for more detail on this topic see *e.g.* [13]). Furthermore, a more correct estimation of the advection time step should consider the local intensity of the velocity gradient; however, following this procedure Δt_a would vary during the time evolution making the time integration more complex and possibly deteriorating the robustness of the scheme. For the Reynolds cell numbers discussed in this work, the constraint on the advection step is generally more restrictive than the one related to the diffusion process. This means that during a time interval Δt_d more than one advection step can be performed. This is true especially far from the boundary layer regions where coarser spatial discretizations and large $\mathrm{Re}_{\Delta r}$ are used. In order to synchronize diffusion and advection steps, Δt_a is arranged so that $\Delta t_d/\Delta t_a$ are an integer ratio (see [2] for more details).

Regarding the SPH method, in its original weakly-compressible formulation, two sta-

https://doi.org/10.4208/cicp.150915.170316a Published online by Cambridge University Press

bility constraints need to be handled:

$$\begin{cases} \Delta t_d \leq K_d \dfrac{\epsilon^2}{\nu} & \Rightarrow \quad \Delta t_d \dfrac{U}{L} \leq K_d \left(\dfrac{\epsilon}{L}\right)^2 \mathrm{Re}, \\ \Delta t_c \leq K_c \dfrac{(2\epsilon)}{c_{sound}} & \Rightarrow \quad \Delta t_c \dfrac{U}{L} \leq K_c \left(\dfrac{2\epsilon}{L}\right) \dfrac{U}{c_{sound}}, \end{cases} \tag{3.4}$$

where the first one is the diffusive-viscous constraint and the second one the acoustic constraint linked to the fictitious speed of sound c_{sound} used in the model.

It is important to note that in SPH for both the acoustic and the diffusive constraints the main parameter is the smoothing length ϵ and not the particle size Δr. This feature is shared with the DVH diffusive time step where the main parameter is the the diffusive radius R_d (see Eq. (3.1)).

A theoretical analysis of the constraints (3.4) has been recently provided by [46] where it has been also shown that the choice of the kernel shape used in the SPH model has not a great influence on the CFL parameters K_d and K_c, if a specific kernel parameter σ is considered instead of the classical smoothing length ϵ.

Here, for the sake of simplicity, heuristic values for the parameters K_d,K_c have been used, which have been obtained after several numerical tests on different benchmarks (see *e.g.* [26, 40, 47, 48]). In particular a fourth order Runge-Kutta time integrator is considered, together with a Wendland C2 kernel with a support equal to $R_w = 2\epsilon$.

In such conditions the two CFL values are:

$$K_d = 0.125, \qquad K_c = 1.0,$$

where the first value was used also in [38] based upon the usual condition for an explicit finite difference method simulating diffusion processes. Note that $R_d = R_w = 2\epsilon$ for both DVH and SPH. This means that for DVH a K_d equal to 0.084 results from Eq. (3.2) against a value of 0.125 for the SPH, which may be assumed a negligible difference from a practical point of view. With the above CFL constants the ratio between the diffusive and the acoustic time step is:

$$\frac{\Delta t_d}{\Delta t_c} = \frac{1}{16}\mathrm{Re}_0, \qquad \mathrm{Re}_0 := \frac{\epsilon c_{sound}}{\nu} = \left(\frac{\epsilon}{\Delta r}\right)\frac{\mathrm{Re}_{\Delta r}}{\mathrm{Ma}} \tag{3.5}$$

being Re_0 a numerical local Reynolds number used in the analysis performed in [46]. Considering that:

(i) the Mach number $\mathrm{Ma} := U/c_{sound} = 0.1$ is the upper limit for the weakly-compressible hypothesis;

(ii) the Reynolds cell number $\mathrm{Re}_{\Delta r}$ in practical simulation is $\mathcal{O}(1)$;

(iii) the ratio $\epsilon/\Delta r$ ranging between 2 and 8,

https://doi.org/10.4208/cicp.150915.170316a Published online by Cambridge University Press

the Δt_d is generally one order higher (or even more) than the acoustic one (unless very high viscous flows are simulated, i.e. $\mathrm{Re}_{\Delta r} \ll 1$).

Besides these two stability constraints, also for the SPH a limit on the time step for the advection of the particles should be considered. Indeed, the SPH is even more sensitive to the particle spatial distribution than the DVH (see *e.g.* [10]) therefore the constraints (3.4) need to be completed with:

$$\begin{cases} \Delta t_a = \mathrm{K}_2 \dfrac{\Delta r}{U} \;\Rightarrow\; \Delta t_a \dfrac{U}{L} = \mathrm{K}_2 \dfrac{1}{L/\Delta r}, \\ \Delta t_{\mathrm{SPH}} \leq \min(\Delta t_d, \Delta t_c, \Delta t_a), \end{cases} \tag{3.6}$$

where K_2 is generally smaller than the K_1 used for the DVH. Similarly to the DVH, this third SPH constraint is needed only for accuracy purposes and not for stability reasons.

To compare the three different time steps, Eqs. (3.4) and (3.6) can be rearranged as:

$$\begin{cases} \Delta t_d \dfrac{U}{L} = K_d \left(\dfrac{\epsilon}{\Delta r}\right)^2 \dfrac{\mathrm{Re}}{(L/\Delta r)^2}, \\ \Delta t_c \dfrac{U}{L} = K_c \left(\dfrac{2\epsilon}{\Delta r}\right) \dfrac{\mathrm{Ma}}{L/\Delta r}, \qquad \Delta t_{\mathrm{SPH}} \leq \min(\Delta t_d, \Delta t_c, \Delta t_a). \\ \Delta t_a \dfrac{U}{L} = \mathrm{K}_2 \dfrac{1}{L/\Delta r}, \end{cases} \tag{3.7}$$

If $\epsilon/\Delta r = 2$, $\mathrm{Ma} = 0.1$ and the constant K_2 is fixed to 0.3, Eq. (3.7) becomes:

$$\begin{cases} \Delta t_d \dfrac{U}{L} = 0.5 \dfrac{1}{L/\Delta r} \mathrm{Re}_{\Delta r}, \\ \Delta t_c \dfrac{U}{L} = 0.4 \dfrac{1}{L/\Delta r}, \\ \Delta t_a \dfrac{U}{L} = 0.3 \dfrac{1}{L/\Delta r}. \end{cases} \tag{3.8}$$

With this choice, considering values of the Reynolds cell number $\mathrm{Re}_{\Delta r}$ of order $\mathcal{O}(1)$, the most restrictive time step for the SPH is the advective one as for the DVH model.

The above practical consideration is rarely commented in the SPH literature where only the stability constraints (3.4) are generally taken into account. This can lead to a wrong deduction that the weakly compressible SPH scheme is limited by small time steps because of the high value of the speed of sound c_{sound} (see *e.g.* [49, 50]), while actually the most critical restraint is linked to the advection of the particles as in the case of the Incompressible SPH models or the Moving Particle Semi-implicit ones. Clearly, if Mach numbers lower than 0.1 are considered the acoustic constraint becomes the most stringent for the SPH, as for example in water impacts (see [51]).

https://doi.org/10.4208/cicp.150915.170316a Published online by Cambridge University Press

This section is concluded considering flows dominated by strong accelerations. Indeed as commented in [38] a time step constraint based on the expected maximum acceleration, $a_{\max}$, should be also considered. As commented in Section 2, differently from the VPM the SPH equations are expressed in terms of particle acceleration; hence, the advective constraint should be rewritten as:

$$\frac{1}{2}a_{\max}\Delta t_a^2 + U\Delta t_a \leq \Delta r, \tag{3.9}$$

the above constraint can be reformulated as:

$$a_{\max}\Delta t_a^2 + 2U\Delta t_a = K_3^2\Delta r, \tag{3.10}$$

where K_3 is a new constant for the advection constraint small enough to guarantee (3.9). Solving the second order equation (3.10) we get:

$$\Delta t_a = U\frac{\sqrt{1+\alpha^2}-1}{a_{\max}}, \qquad \alpha := K_3\frac{\sqrt{a_{\max}\Delta r}}{U}. \tag{3.11}$$

Considering the condition $\alpha \ll 1$ Eq. (3.11) becomes the last equation of (3.7) with $K_3 = \sqrt{2K_2}$. Vice-versa if α is much larger than one, or in other words the flow is dominated by strong accelerations, the above equation can be simplified as:

$$\Delta t_a = K_3\sqrt{\frac{\Delta r}{a_{\max}}} \quad \Rightarrow \quad \Delta t_a\frac{U}{L} = K_3\sqrt{\frac{U^2}{La_{\max}}}\frac{1}{\sqrt{L/\Delta r}}, \tag{3.12}$$

which is the relation written in [38] when the constant K_3 is set equal to 0.3 and the maximum acceleration is evaluated as the maximum acceleration among the particles $a_{\max} = \max_i(\mathbf{a_i})$. It is interesting to underline that considering larger and larger ratios $L/\Delta r$, the constraint (3.12), because of its dependency on $\sqrt{\Delta r}$, becomes less restrictive than the last constraint of (3.8).

4 Numerical results

In the present section two test-cases are considered:

- the free-vorticity dynamics of a single Lamb-Oseen vortex,
- the vortex shedding around an inclined ellipse at Re$=$500.

The two test-cases are simulated both with DVH and SPH methods.

The first problem can be demanding for the SPH method because it is mainly dominated by the viscous forces. Since SPH is based on low order integral interpolation formulae, the error on second order operators is quite sensitive to the particle disorder. To

https://doi.org/10.4208/cicp.150915.170316a Published online by Cambridge University Press

limit this error, the number of particles inside the support of the kernel W needs to be large enough (high ratios $\epsilon/\Delta r$).

For the second test-case, an intense rolled up mechanism in the wake region is expected developing a regular periodic shedding after a transitory stage. The spatial resolution adopted for both methods is $c/\Delta r=200$, where c is the major axis of the ellipse, in order to resolve the smallest spatial vorticity scales. In this second case inflow/outflow boundaries need to be handled in the SPH model while they are automatically enforced within the DVH model. Since this problem represents a more practical application from an engineering point of view, an analysis of the CPU costs involved in the two models has been carried out.

4.1 Lamb-Oseen Vortex test case

The Lamb-Oseen vortex is a solution of the incompressible N.S. equations in an unbounded domain for an initial velocity field, in polar coordinates, equal to:

$$\boldsymbol{u}_0(r)=\omega_0\frac{L^2}{2r}\left[1-e^{-(r/L)^2}\right]\hat{\theta}, \tag{4.1}$$

where L is the length scale of the problem and $\hat{\theta}$ the normal tangential unit vector.

The corresponding initial vorticity distribution is equal to:

$$\omega(r,0)=\omega_0 e^{-(r/L)^2}, \tag{4.2}$$

being ω_0 the vorticity in $r=0$ at $t=0$.

During the evolution the velocity field remains purely tangential and the vorticity field maintains a Gaussian shape:

$$\omega(r,t)=\omega_0 f(t)e^{-f(t)(r/L)^2},\quad f(t):=\frac{\mathrm{Re}}{4\pi t\omega_0+\mathrm{Re}}. \tag{4.3}$$

Furthermore, for this problem the convective term of the acceleration is null in the tangential direction:

$$[\nabla\boldsymbol{u}\boldsymbol{u}]\cdot\hat{\theta}=0\quad\Rightarrow\quad[\boldsymbol{a}(\mathbf{r},t)]\cdot\hat{\theta}=\left[\frac{D\boldsymbol{u}(\mathbf{r},t)}{Dt}\right]\cdot\hat{\theta}\equiv\left[\frac{\partial\boldsymbol{u}(\mathbf{r},t)}{\partial t}\right]\cdot\hat{\theta}, \tag{4.4}$$

where $\boldsymbol{a}$ is the fluid particle acceleration. Eulerian mesh-based solver formulated in polar coordinates can benefit from this property in solving this flow. Indeed, for these methods the variation of the Reynolds number implies just a change in the time scale, leaving the numerical error unchanged for a given resolution (in the $\hat{\theta}$ direction the N.S. equations become a simple linear heat equation uncoupled from the radial direction, for details see *e.g.* [42]).

This is not the case for Lagrangian solvers where the particles are directly advected with a certain level of numerical errors which depends on the selected Reynolds number.

https://doi.org/10.4208/cicp.150915.170316a Published online by Cambridge University Press

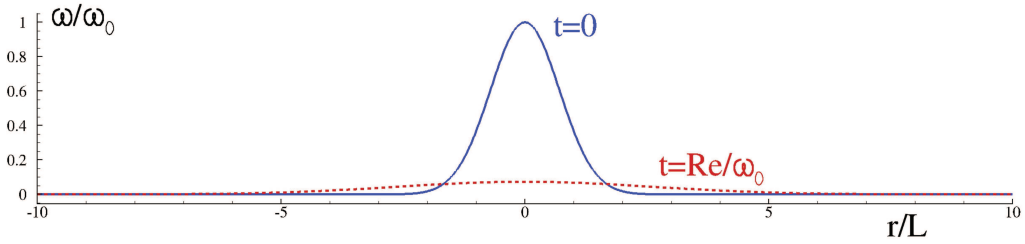


Figure 5: Lamb-Oseen vortex problem: vorticity profiles at $t=0$ (solid line) and $t=\mathrm{Re}/\omega_0$ (dashed line).

A similar test case can be the Taylor-Green vortex widely used to validate SPH solvers (see *e.g.* [10, 44, 52–54]). However this test-case has the disadvantage to become unstable at moderate Reynolds number while the Lamb-Oseen Vortex has a wider stability range when decreasing the viscosity level.

For the sake of brevity the complete solution of Lamb-Oseen Vortex in terms of velocity and pressure fields is not reported here and can be found in [2]. Knowing the analytical solution, such a simple problem can be used to measure heuristically the convergence of DVH and SPH when varying the Reynolds number. Thus, a relative error E_f for the generic function $f(x,t)$ is defined using a combination of L_1 norm in space and L_∞ in time:

$$E_f = \max_{t\in(0,t_{end}]} \frac{\int_\Omega |f_{\text{exact}}(x,t)-f(x,t)|dx}{\int_\Omega |f_{\text{exact}}(x,t)|dx}, \tag{4.5}$$

where Ω is the computational fluid domain. The latter is defined as a circular domain with radius $R=20L$; in this way Ω is large enough to ensure that the vorticity field is practically negligible on $\partial\Omega$.

The final time, t_{end}, is set equal to Re/ω_0. In this time range the maximum vorticity in Ω is reduced to about 7% of the initial value ω_0. In the analytical solution Re simply changes the time scale. However, when increasing the Reynolds number the advection step becomes more and more important introducing errors in Lagrangian particle methods. Fig. 6 shows the fluid deformation for two different Reynolds numbers, 100 and 1000, during the same time range $t\in[0,\mathrm{Re}/\omega_0]$.

Since in the DVH the boundary condition at infinity is automatically satisfied, there is no need to confine the fluid domain Ω. The vorticity field is discretized only for $r\leq R$, with $R=20L$ while beyond this distance the vorticity is neglected because of its small values. Conversely, the SPH method requires a closed domains and this is realized by considering an annular region $r\in(R,R+R_w)$ where fictitious equispaced particles are positioned and where values for u and p are prescribed. Furthermore, in order to avoid the excitation of the so-called tensile instability in the SPH method, a positive constant pressure $P=\rho_0\omega_0^2L^2\log(2)/4$ is used.

Left plot of Fig. 7 shows the behaviours of the SPH error on the velocity fields, E_u, for various ratios L/R_w and $R_w/\Delta r$. Using the ratio $R_w/\Delta r=2$, which corresponds to only 13 interacting neighbours, the SPH does not converge for any spatial resolution L/R_w.

https://doi.org/10.4208/cicp.150915.170316a Published online by Cambridge University Press

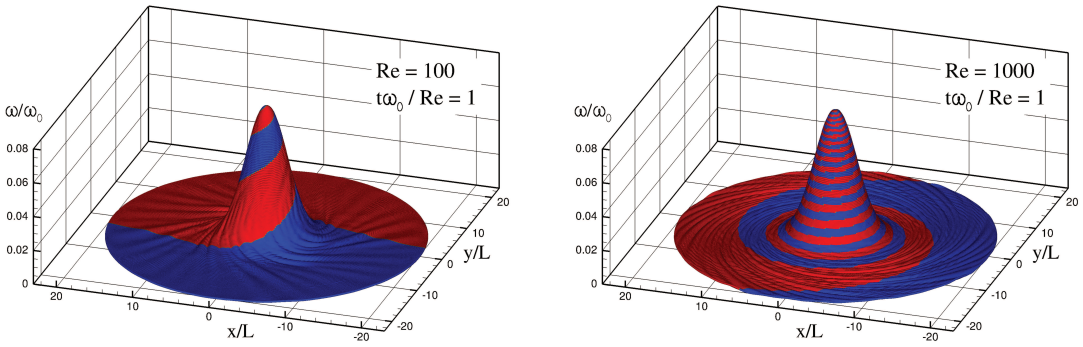


Figure 6: Fluid deformation for the Lamb-Oseen problem for two different Reynolds numbers. Particles coloured in blue were initially positioned on $x<0$ semi-plane while red particle belonged to $x>0$ at $t=0$. Vertical axis represents the vorticity intensity.

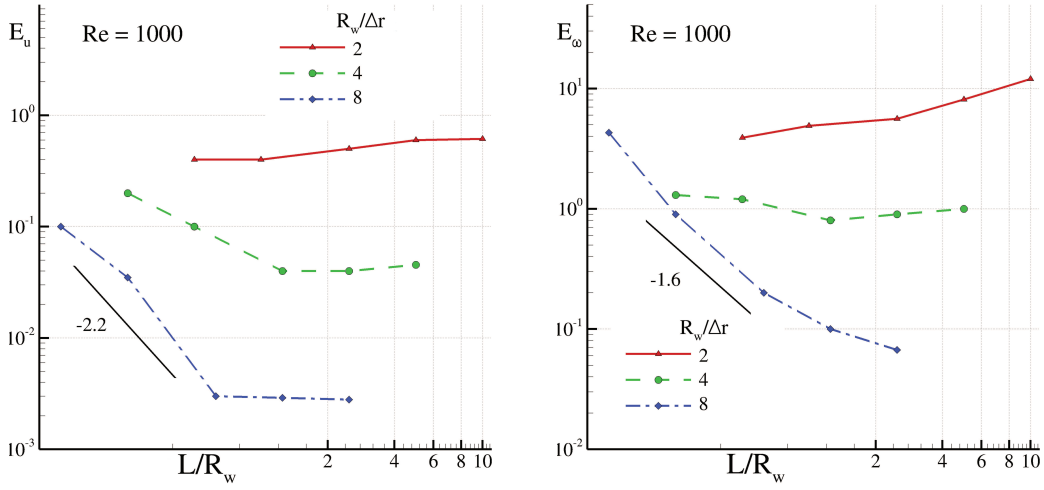


Figure 7: Lamb-Oseen vortex at Re$=1000$: SPH errors on the velocity field E_u (left) and on the vorticity field E_ω using three different ratios $R_w/\Delta r=2$, 4, 8.

For the ratios $R_w/\Delta r=4,8$ (corresponding to a number of neighbours of 50 and 200 in the kernel support) and for the first three spatial resolution the solver converges with a ratio close to 1 and 2 respectively; then a saturation level is reached for the two last points. This is in agreement with the theoretical analysis performed by [7] where the role of the "smoothing error" and the "discretization error" (i.e. the error made in the discretization of the integral interpolation) is discussed: when the discretization error becomes significant with respect to the smoothing error a saturation regime appears. From that theoretical analysis, confirmed by the results presented in Fig. 7, it results that in order to decrease the SPH errors both the ratios $\Delta r/\epsilon$ and $\Delta r/L$ need to be reduced.

Right plot of Fig. 7 shows the SPH error for the vorticity field, E_ω, which is not a primary variable and needs to be calculated by a further smoothing procedure from the velocity field. This explains why E_ω presents higher error levels with respect to E_u.

https://doi.org/10.4208/cicp.150915.170316a Published online by Cambridge University Press

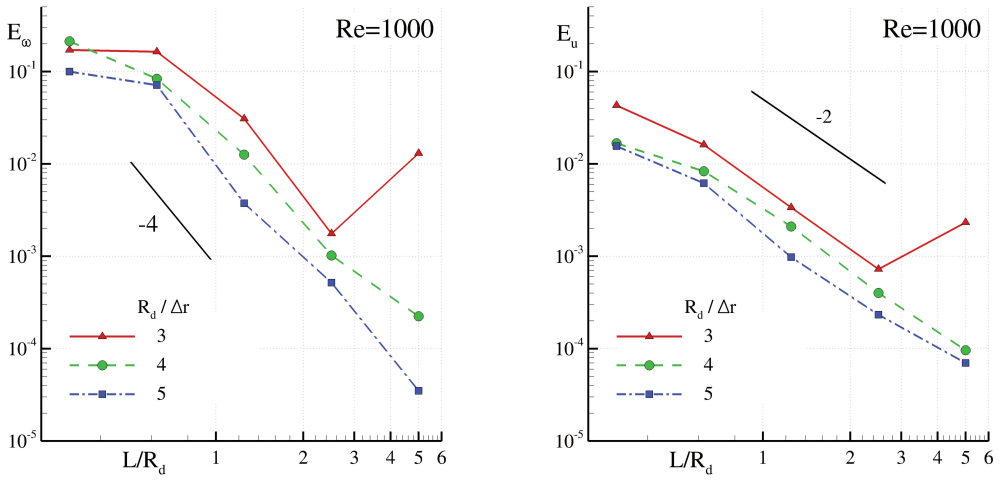


Figure 8: Lamb-Oseen vortex at Re$=$1000: DVH errors on the vorticity field E_ω (left) and on the velocity field E_u (right) using three different ratios $R_d/\Delta r=3$, 4, 5.

In practice a convergence for the vorticity is only visible using $R_w/\Delta r=8$; indeed, for lower ratios spurious numerical vorticity starts to form, inducing errors in the numerical solution. The development of this "numerical turbulence" and its connection to extra-dissipation mechanism has been already commented in [40] in the context of viscous gravity waves.

Regarding the DVH, also for this method we have two main parameters for studying the convergence: (i) the spatial resolution L/R_d and (ii) the ratio $R_d/\Delta r$. Therefore, the diffusive radius plays the same role of the kernel support R_w for the SPH. Left plot of Fig. 8 depicts the errors on the vorticity E_ω for the DVH model. Main differences with the SPH are: E_ω is two order of magnitude smaller, the rate of convergence being much higher. Beside this, it is remarkable that for the smallest ratio $R_d/\Delta r$ an error saturation at the highest resolution is observed. Increasing $R_d/\Delta r$ the level of error decreases again. Even if the rate of convergence is close to 4 for E_ω, the error on the velocity field E_u shows a second order convergence with levels of error close to E_ω for spatial resolution $L/R_d>1$.

Fig. 9 reports the DVH errors E_ω and E_u for Reynolds number equal to 100. As expected, at this larger viscosity level, errors of order 10^{-4} are reached with a coarser spatial resolutions with respect to the Re$=$1000 case. For Re$=$100 the DVH plots become more similar to the ones obtained with the SPH at Re$=$1000. Indeed, here the "discretization error" becomes dominant for the DVH since the error related to the solution of the diffusion process is higher than the one linked to the advection one.

While E_ω exhibits a saturation of the error levels for all the ratios $R_d/\Delta r$, on the velocity field the saturation is present only at the smallest ratio $R_d/\Delta r=3$. For the two highest ratio $R_d/\Delta r$, E_u always shows a convergence rate close to second order, at least for the simulations here considered.

https://doi.org/10.4208/cicp.150915.170316a Published online by Cambridge University Press

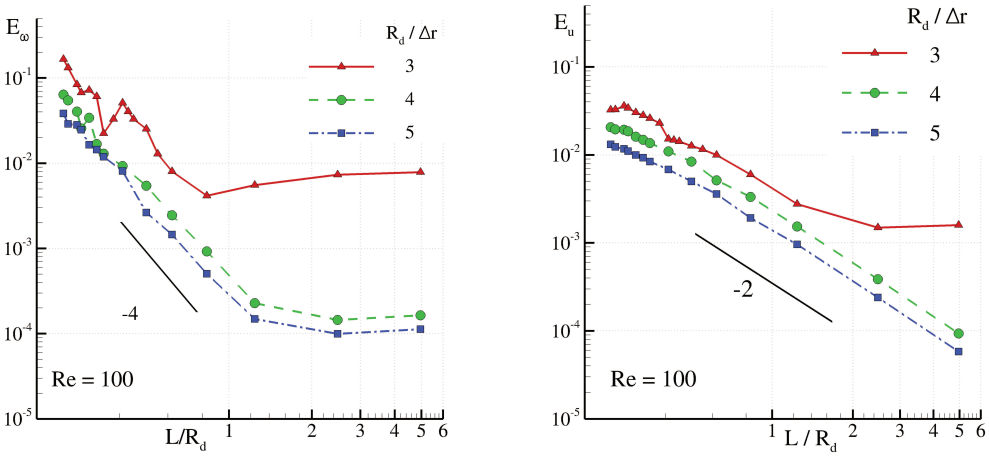


Figure 9: Lamb-Oseen vortex at Re$=100$: DVH errors on the vorticity field E_ω (left) and on the velocity field E_u (right) using three different ratios $R_d/\Delta r=3$, 4, 5.

4.2 Flow around an inclined elliptical cylinder Re$=500$

A series of simulations of the viscous flow around an elliptical cylinder with axis ratio 0.4 and angle of attack $\alpha=20$ is performed at Re$=500$. An example of the DVH vorticity field is shown in top plot of Fig. 10 for $c/\Delta r=200$ (where c is the major axis and Δr the mean distance among the particles close to the solid body).

For the SPH the model described in [47] has been used, with an artificial diffusive term added on the continuity equation (δ-SPH) and a ghost-particle technique used to enforce the no-slip boundary condition on the ellipse surface. In the SPH simulation an inlet and outlet boundaries are needed for this kind of flow (see *e.g.* [55]). The inlet boundary is positioned at $x=-4c$ while the outlet boundary is positioned at $x=12c$. The spatial resolution is uniform in the whole domain, and the latter is confined by two lateral walls at $y=\pm 4c$ where a free-slip boundary condition is enforced. The total number of particles used is 5,100,000.

Differently to the SPH, in the DVH method the inlet condition is automatically achieved by the potential solver while instead of using an outlet frontier a multi-resolution technique is used in order to gradually degrading the spatial resolution up to $c/\Delta r=25$ in the far field region $x\in(10c,50c)$. Therefore, when particles enter in the far field they are merged in large vortices during the diffusion process (details of this technique are reported in [3]). At the final time $t_f U/c=40$ the total number of vortex particles is 425,000 one order of magnitude smaller than the number of particles used in the SPH.

We underline that the spatial resolution $c/\Delta r$ is equal to 200 for both the methods, however, for the DVH only the region with non-zero vorticity is discretized while for the SPH the whole fluid domain needs to be discretized with particles. On the other hand, as discussed in the following, the CPU cost per particle can be higher in the DVH than

https://doi.org/10.4208/cicp.150915.170316a Published online by Cambridge University Press

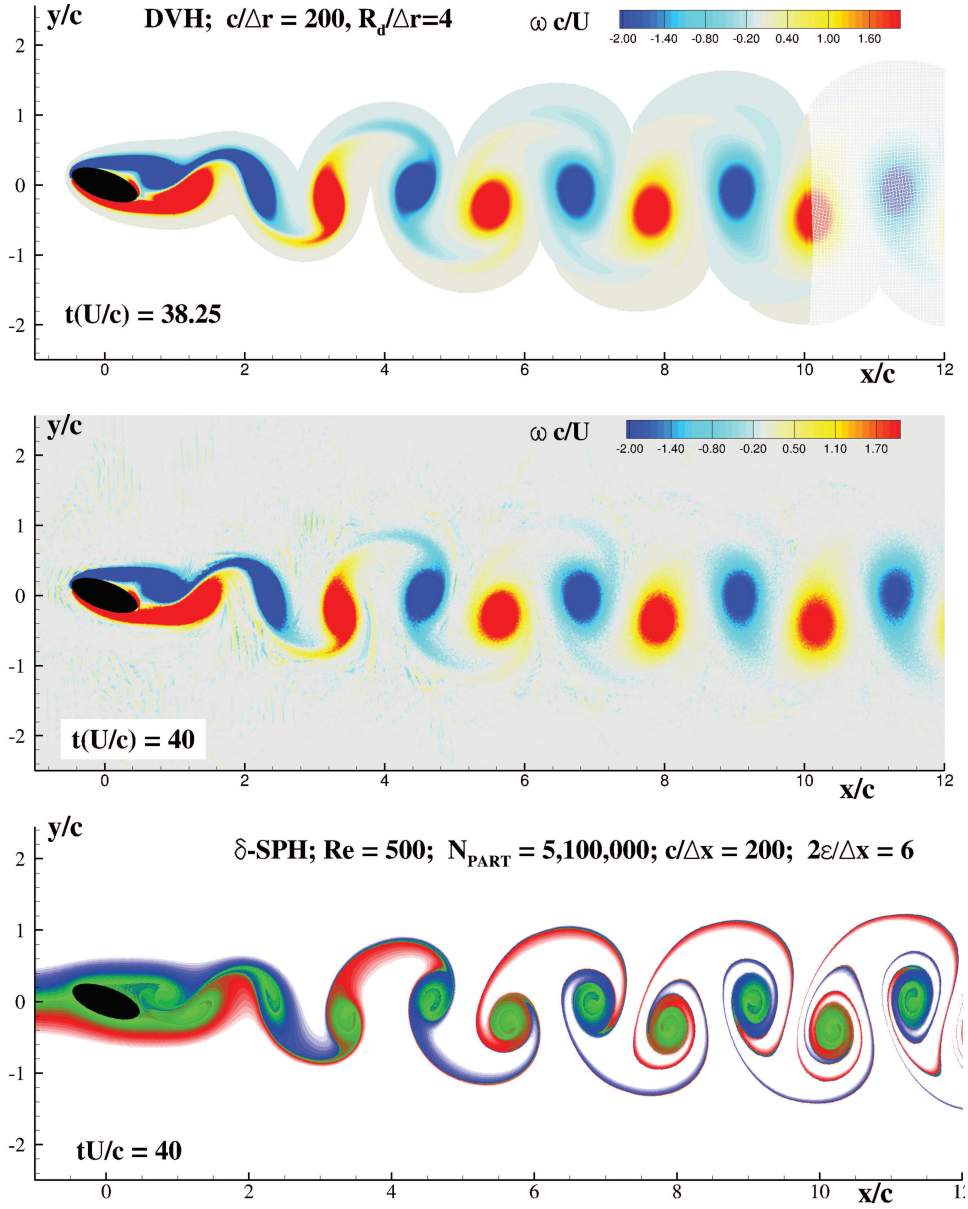


Figure 10: Flow around an inclined elliptical cylinder: DVH vorticity field (top), SPH vorticity field (middle), SPH streaklines (bottom).

in the SPH solver. Furthermore, from the point of view of memory requirement, the SPH solver generally needs more memory than the DVH.

Middle plot of Fig. 10 depicts the SPH vorticity field which is very close to the DVH one but for small numerical noise mainly given by the particle rearrangement during the

https://doi.org/10.4208/cicp.150915.170316a Published online by Cambridge University Press

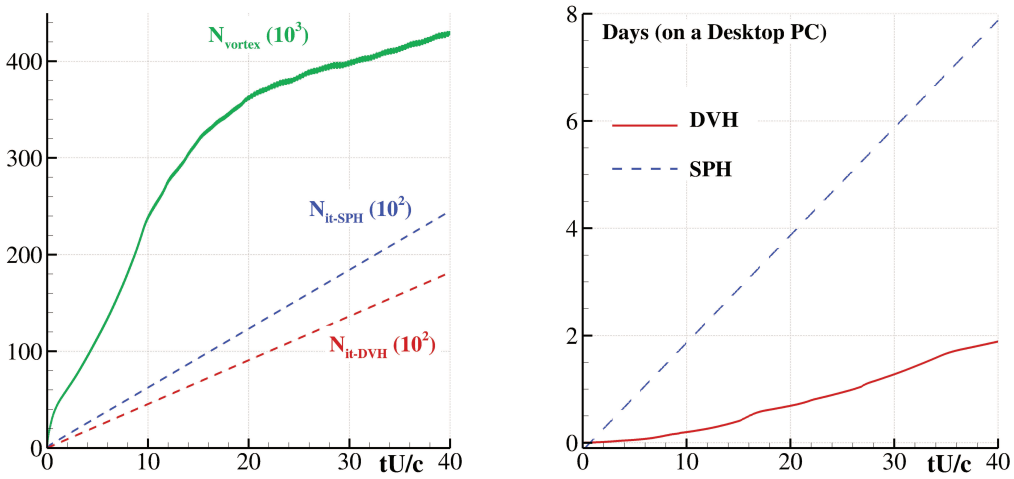


Figure 11: Flow around an inclined elliptical cylinder. Left: time history of the number of vortex particles that are shed in the DVH (solid line); SPH and DVH time iterations (dashed lines). Right: CPU costs for DVH and SPH. The spatial resolution for both the solvers is $c/\Delta r = 200$.

evolution. It is important to underline that the SPH solution has been obtained with a ratio $R_w/\Delta r = 6$ which corresponds to a number of neighbours of about 100. In fact for ratio $R_w/\Delta r = 4$, often adopted by SPH practitioners, the vorticity field becomes much more disturbed as already commented for the results on the Lamb-Oseen test-case. The bottom plot of Fig. 10 shows the SPH streaklines which are directly drawn from the particle indexes; this operation is not possible with the DVH for which a set of Lagrangian markers should be added in the solver and integrated in time. This would imply an increase of the CPU costs because velocity should be evaluated not only on the vortex particles but also on Lagrangian markers.

Left plot of Fig. 11 shows the time history of the number of vortex particles that are shed when using the DVH method. Thanks to the adopted multi-resolution technique this number remains limited even for long simulation time. Indeed, in the first time range the number of vortices increases almost linearly but when the wake enter in the far-field the vortices are merged in coarser distributions reducing the steepness of $N_{vortex}(t)$. In the same plot the time iterations are also reported. Even if a weakly-compressible model is used for the SPH, the time steps adopted by the two solvers are not so different. Indeed, for the SPH, using a 4th-order Runge-Kutta scheme, and a ratio $\epsilon/\Delta r = 3$ the time step for the compressibility stability constraint (see Section 3) is given by:

$$\Delta t_c \frac{U}{c} = \frac{(2\epsilon)}{c_{sound}} \frac{U}{c} = 6\frac{\Delta r}{c}\mathrm{Ma} = 0.6\frac{1}{(c/\Delta r)} \tag{4.6}$$

being c the ellipse major axis, c_{sound} the speed of sound adopted for the SPH and Ma the related Mach number (set equal 0.1). Conversely, for the advective time step the CFLs

https://doi.org/10.4208/cicp.150915.170316a Published online by Cambridge University Press

used are:

$$\Delta t_a^{\text{SPH}} \frac{U}{c} = 0.3 \frac{1}{(c/\Delta r)}, \qquad \Delta t_a^{\text{DVH}} \frac{U}{c} = 0.4 \frac{1}{(c/\Delta r)}. \tag{4.7}$$

For the present parameter choice, as already pointed out in Section 3, the latter constraint is the most severe one also for the SPH.

The right plot of Fig. 11 reports the DVH and SPH CPU costs for the present test-case using the highest spatial resolution $c/\Delta r = 200$. For both solvers a desktop PC six cores Xeon(R) CPU X5650, 2.3GHz has been used; a simple OpenMP parallel programming has been adopted.

The CPU cost of the DVH solver is about $100\mu s$ per vortex particle and per time iteration on a single core, while for the SPH solver the cost is about $50\mu s$ per particle and per time iteration on a single core (using 100 interacting neighbours). For the performed computations the SPH took about 8 days of calculation versus the two days of the DVH, with a memory occupation ten times larger. However, it should be noted that SPH is more flexible in terms of range of applicability: for example the introduction of a free surface in this viscous flow (see *e.g.* [56]) or an air/water interface is practically trivial while it is not the case for any Vortex Particle Method.

Left plot of Fig. 12 shows the time histories of the drag force predicted by the SPH using three different spatial resolutions $c/\Delta r =$ N, 2N, 4N with $N = 50$. To evaluate the convergence properties on the drag evaluation the difference between the time histories of two different spatial resolutions, $c/\Delta r = 2N$ and N, is calculated as:

$$\Delta\mathcal{E}_{2N,N} := \left[\int_0^{t_f} \left|C_{d,2N} - C_{d,N}\right| dt\right] \left[\int_0^{t_f} \left|C_{d,N_{\text{MAX}}}\right| dt\right]^{-1}, \tag{4.8}$$

where N_{MAX} is the maximum spatial resolution adopted (in our case $N_{\text{MAX}} = 200$).

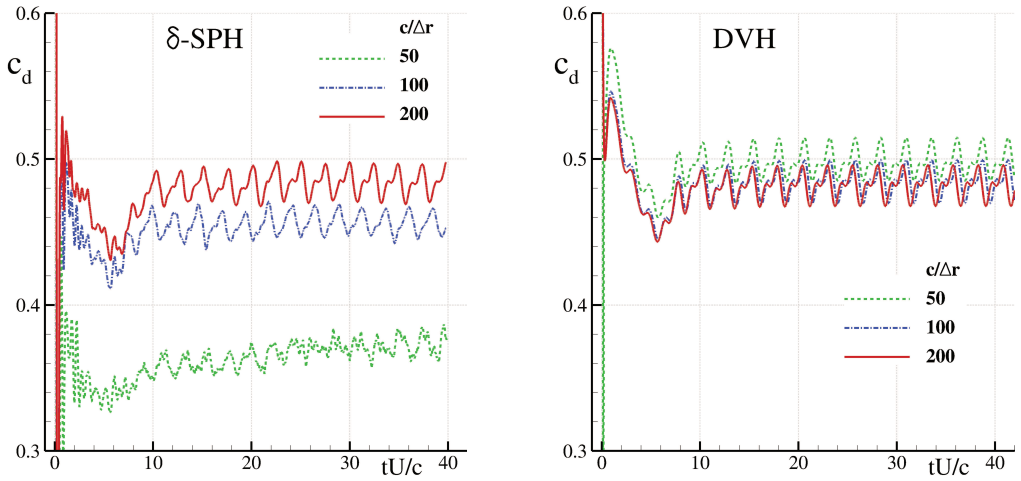


Figure 12: Flow around an inclined elliptical cylinder: time history of the SPH drag coefficient (left) and of the DVH drag coefficient (right) for three different spatial resolutions.

https://doi.org/10.4208/cicp.150915.170316a Published online by Cambridge University Press

Table 2: Convergence of the DVH and SPH solver for the drag coefficient evaluating using three different spatial resolution: $c/\Delta r = 50,\ 100,\ 200$.

C_d	$\Delta\mathcal{E}_{200,100}$	$\Delta\mathcal{E}_{100,50}$	Ord	Uncert
DVH	0.0312	0.0115	1.44	0.4%
SPH	0.199	0.0887	1.17	3.8%

The SPH drag forces converge with a rate of about 1.2. For the lowest resolution the C_d is quite underestimated because of the large errors in the prediction of the viscous stresses on the cylinder surface. Right plot of the same figure shows the C_d time histories evaluated by the DVH with the same spatial resolutions. The rate of convergence for the DVH is about 1.4. However, even with the coarsest resolution the DVH predicts the viscous forces within a relative error of about 3% with respect to the highest resolution (see Table 2). The obtained uncertainties are, respectively, 3.8% for the SPH and 0.4% for the DVH. The convergence ratios is less than two even for the DVH because the complete time histories are taken into account. Conversely, if only the maximum C_d values are taken into account in the periodic regime, the ratios rise to 1.8 (SPH) and 2.0 (DVH).

Fig. 13 sketches the time history of the lift force evaluated through SPH and DVH with the spatial resolution $c/\Delta r = 200$. As expected the lift forces after a transitory stage, starts to oscillate around a positive mean value. The DVH and SPH are in a good agreement but for the Strouhal frequency, the small differences being mainly due to the blockage effect of the confined domain adopted for the SPH.

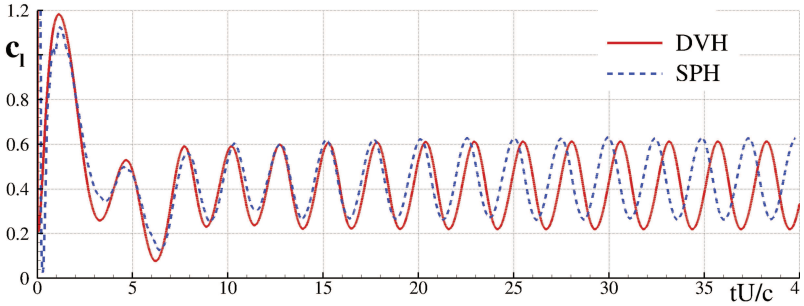


Figure 13: Flow around an inclined elliptical cylinder: time evolution of the lift force coefficient predicted by SPH and by DVH.

5 Discussion on similarities/differences between SPH and DVH

Considering the analysis presented in the previous sections, here a final discussion on similarities/differences between the two particle methods is concisely given through two bulleted lists. These considerations are then supported by the numerical investigation shown in Section 4.

https://doi.org/10.4208/cicp.150915.170316a Published online by Cambridge University Press

Main similarities between SPH and DVH are:

1. SPH and DVH are both Meshless Lagrangian Particle methods:
   (i) the particles are advected according to the evaluated velocity field;
   (ii) the acceleration (SPH) and the velocity (DVH) fields are calculated through convolutions integral with specific Kernel functions.
2. When solving inviscid flows both methods suffer in term of stability and robustness.
3. At least from a theoretical point of view both SPH and DVH can conserve accurately the circulation of material loops.
4. Both methods use an explicit time integration for the particles evolution.
5. The time step constraints are comparable when solving similar flows.
6. When solving viscous flows for moderate and high Reynolds numbers, the more severe time step constraint is generally linked to the particle advection for both the methods.
7. Both the methods are not suitable for solving high viscous flows, because of the explicit time integration.
8. When using the same discretization parameters, $L/\Delta r$ and the radii R_d (DVH) and R_w (SPH), to simulate the same problem, the resulting error levels of the two methods can be quite different. However, the convergence behaviour changing these parameters is the same in both the models, i.e. with some combinations of these parameters a saturation condition can be reached and the solvers do not converge for a further increase of the resolution. The actual values of $L/\Delta r$ and $R_d/\Delta r$, $R_w/\Delta r$ where the saturation occurs depends on the problem and on the considered variable. Furthermore in the regions of convergence, the SPH/DVH convergence ratios can be different.

Main differences between SPH and DVH are:

1. the DVH is a vortex method solving directly the vorticity field, while the SPH method is formulated through pressure and velocity fields. This implies that:
   (i) The accuracy on the velocity/vorticity fields is much higher with the DVH than with the SPH models.
   (ii) DVH requires the discretization of the only vortical regions, but, on the otherhand, a potential flow problem needs to be numerically solved in order take into account the presence of non-permeable boundaries.
2. DVH is formulated for incompressible flows while SPH is generally formulated in the context of compressible flows.

https://doi.org/10.4208/cicp.150915.170316a Published online by Cambridge University Press

3. Because of the different behaviours of the kernel adopted in the SPH and DVH models, distinct algorithms for the particle interactions are needed.
4. The management of multi-resolution domains is more simple in the DVH framework than in the SPH one.
5. For the DVH model the boundary conditions at infinity are automatically satisfied, while with the SPH large spatial domains are required to correctly enforce them.
6. Thanks to the diffusion process on a regular distribution of geometrical points, DVH does not suffer from irregularities on the particles spatial distributions.
7. With the SPH method it is much easier to take into account fluid particles having different physical properties (*e.g.* multiphase flows, particle-laden flows, magnetohydrodynamics, etc.)
8. SPH method can be directly applied to the context of free-surface flows [57, 58] while this is not the case for the DVH where a specific treatment of air-water interface is needed.

6 Conclusions

This work is dedicated to two different particle methods: the Smoothed Particle Hydrodynamics (SPH) and the Diffused Vortex Hydrodynamics (DVH). The latter is a Vortex Particle Method (VPM) recently developed to simulate complex viscous flows in the medium and high Reynolds regimes. DVH and SPH methods present some similarities because of their Lagrangian meshless nature, even if they are based on different numerical approaches.

Advantages and drawbacks of the two methods have been studied in previous works and further investigations are discussed in the present article highlighting analogies and differences.

A first comparison has been provided in the context of inviscid flows (Euler equation) discussing the role of the smoothed approximation of the main fields and the related kernel functions for the evaluation of the particle interactions. Then the treatment of the viscosity diffusion process is considered in the two models. In particular the DVH solution for the vorticity diffusion presents strong analogies with the SPH smoothing procedure.

Furthermore, some crucial aspects of the time integration schemes are discussed from theoretical and numerical point of views. Conversely to what generally claimed in the SPH literature, the advection time step resulted the most restrictive one not only for the DVH but also for the SPH in the considered simulation conditions.

These different aspects are finally investigated through two dedicated numerical test-cases showing that, due to those analogies, DVH and SPH present similar convergence behaviours. However, the error levels depend on the quantity under consideration and

https://doi.org/10.4208/cicp.150915.170316a Published online by Cambridge University Press

can be quite different when fixing similar particle sizes Δr and the radii R_d (DVH), R_w (SPH).

Acknowledgments

Work supported by Flagship Project RITMARE – Italian Research for the Sea – coordinated by Italian National Research Council and funded by Italian Ministry of Education, University and Research within Nat. Res. Program 2015-2016, and partially supported by the Project ENSiS: ENhanced Sph Schemes for complex free-surface flows, funded by the Ecole Centrale de Nantes (ECN).

References

[1] A. Colagrossi, G. Graziani, and M. Pulvirenti, Journal of Mathematics and Mechanics of Complex Systems **2**, 45 (2014).
[2] E. Rossi, A. Colagrossi, and G. Graziani, Computers and Mathematics with Applications **69**, 1484 (2015a).
[3] E. Rossi, A. Colagrossi, B. Bouscasse, and G. Graziani, Communications in Computational Physics **18**, 351 (2015b).
[4] J. U. Brackbill, D. B. Kothe, and H. M. Ruppel, Computer Physics Communications **48**, 25 (1988).
[5] R. Vacondio, B. Rogers, P. Stansby, P. Mignosa, and J. Feldman, Computer Methods in Applied Mechanics and Engineering (2013).
[6] A. Chorin, Journal of Fluid Mechanics **57**, 785 (1973).
[7] N. J. Quinlan, M. Lastiwka, and M. Basa, International Journal for Numerical Methods in Engineering **66**, 2064 (2006).
[8] D. Le Touzé, A. Colagrossi, G. Colicchio, and M. Greco, International Journal for Numerical Methods in Fluids **73**, 660 (2013).
[9] A. M. Tartakovsky and P. Meakin, Journal of Computational Physics **207**, 610 (2005).
[10] M. Antuono, B. Bouscasse, A. Colagrossi, and S. Marrone, Computer Physics Communications **185**, 2609 (2014).
[11] H. Wendland, Adv. Comput. Math. **4**, 389 (1995).
[12] M. Ranucci, Ph.D. thesis, Sapienza, Università di Roma (1995).
[13] G.-H. Cottet and P. D. Koumoutsakos, *Vortex methods: theory and practice* (Cambridge university press, 2000).
[14] J. J. Monaghan, Reports on Progress in Physics **68**, 1703 (2005).
[15] M. Antuono, A. Colagrossi, D. Le Touzé, and J. J. Monaghan, International Journal for Numerical Methods in Fluids **72**, 583 (2013), ISSN 1097-0363.
[16] G. Graziani, M. Ranucci, and R. Piva, Computational mechanics **15**, 301 (1995).
[17] R. Hockney and E. J.W., *Computer simulation using particles* (Adam Hilger, Bristol, 1988).
[18] J. Barnes and P. Hut (1986).
[19] L. Greengard and V. Rokhlin, Journal of Computational Physics **73**, 325 (1987).
[20] D. Price and J. Monaghan, Mon. Not. R. Astron. Soc. **0**, 1 (2003).
[21] A. Marsh, G. Oger, D. Le Touzé, and D. Guibert, in *6th International SPHERIC workshop* (2011), pp. 86–92.

https://doi.org/10.4208/cicp.150915.170316a Published online by Cambridge University Press

[22] D. Barcarolo, D. L. Touzé, G. Oger, and F. de Vuyst, Journal of Computational Physics **273**, 640 (2014).
[23] J. Vila, Mathematical Models & Methods in Applied Sciences **9**, 161 (1999).
[24] J.-C. Marongiu, F. Leboeuf, J. Caro, and E. Parkinson, Journal of Hydraulic Research **48**, 40 (2010).
[25] P. Koukouvinis, J. Anagnostopoulos, and D. E. Papantonis, International Journal for Numerical Methods in Fluids **71**, 1152 (2013).
[26] M. Antuono, A. Colagrossi, and S. Marrone, Computer Physics Communications **183**, 2570 (2012).
[27] J. W. Swegle, D. L. Hicks, and S. W. Attaway, Journal of Computational Physics **116**, 123 (1995).
[28] T. Belytschko and S. Xiao, Computer and Mathematics with applications **43**, 329 (2002).
[29] T. Belytschko, Y. Guo, W. Liu, and S. Xiao, Int. J. Numer. Methods Engineering **48**, 1359 (2000).
[30] P. Randles and L. Libersky, International Journal for Numerical Methods in Engineering **48**, 1445 (2000).
[31] J. Monaghan, J. Comp. Phys. **159**, 290 (2000).
[32] J. Bonet and S. Kulasegaram, Int. J. Numer. Methods Engineering **52**, 1203 (2001).
[33] L. Barba, A. Leonard, and A. C.B., in *16th AIAA Computational Fluid Dynamics Conference* (2003), vol. AIAA 2003-2140.
[34] A. Gharakhani, in *15th AIAA Computational Fluid Dynamics Conference* (2001), pp. 1–10.
[35] M. Benson, P. Bellamy-Knights, J. Gerrard, and I. Gladwell, Journal of Fluids and Structures **3**, 439 (1989).
[36] A. Colagrossi, B. Bouscasse, M. Antuono, and S. Marrone, Computer Physics Communications **183**, 1641 (2012).
[37] J. Monaghan and R. A. Gingold, Journal of Computational Physics **52**, 374 (1983).
[38] J. P. Morris, P. J. Fox, and Y. Zhu, Journal of Computational Physics **136**, 214 (1997).
[39] P. Español and M. Revenga, Phys. Rev. E **67**, 026705 (2003).
[40] A. Colagrossi, A. Souto-Iglesias, M. Antuono, and S. Marrone, Phys. Rev. E **87**, 023302 (2013).
[41] A. Colagrossi, B. Bouscasse, and S. Marrone, Phys. Rev. E **92**, 053003 (2015).
[42] A. Colagrossi, M. Antuono, A. Souto-Iglesias, and D. Le Touzé, Physical Review E **84**, 026705 (2011).
[43] D. Violeau, Phys. Rev. E **80**, 036705 (2009).
[44] S. Lind, R. Xu, P. Stansby, and B. Rogers, Journal of Computational Physics **231**, 1499 (2012).
[45] R. Fatehi and M. Manzari, Computers & Mathematics with Applications **61**, 482 (2011), ISSN 0898-1221.
[46] D. Violeau and A. Leroy, Journal of Computational Physics **256**, 388 (2014).
[47] S. Marrone, A. Colagrossi, M. Antuono, G. Colicchio, and G. Graziani, Journal of Computational Physics **245**, 456 (2013), ISSN 0021-9991.
[48] B. Bouscasse, A. Colagrossi, S. Marrone, and M. Antuono, Journal of Fluids and Structures **42**, 112 (2013).
[49] E. S. Lee, C. Moulinec, R. Xu, D. Violeau, D. Laurence, and P. Stansby, Journal of Computational Physics **227**, 8417 (2008).
[50] D. Violeau and A. Leroy, Journal of Computational Physics **288**, 119 (2015).
[51] S. Marrone, A. Colagrossi, A. Di Mascio, and D. Le Touzé, Journal of Fluids and Structures **54**, 802 (2015).
[52] N. Trask, M. Maxey, K. Kim, M. Perego, M. L. Parks, K. Yang, and J. Xu, Computer Methods

https://doi.org/10.4208/cicp.150915.170316a Published online by Cambridge University Press

in Applied Mechanics and Engineering **289**, 155 (2015).
[53] R. Xu, P. Stansby, and D. Laurence, Journal of Computational Physics **228**, 6703 (2009), ISSN 0021-9991.
[54] R. M. Nestor, M. Basa, M. Lastiwka, and N. J. Quinlan, Journal of Computational Physics **228**, 1733 (2009).
[55] I. Federico, S. Marrone, A. Colagrossi, F. Aristodemo, and M. Antuono, European Journal of Mechanics-B/Fluids **34**, 35 (2012).
[56] B. Bouscasse, A. Colagrossi, A. Souto-Iglesias, and S. Marrone, in *33rd International Conference on Ocean, Offshore and Arctic Engineering (OMAE)*, edited by Asme (2014).
[57] J. Monaghan, J. Comp. Phys. **110**, 39 (1994).
[58] A. Colagrossi, M. Antuono, and D. Le Touzé, Physical Review E **79**, 056701 (pages 13) (2009).

https://doi.org/10.4208/cicp.150915.170316a Published online by Cambridge University Press